Journal of Alloys and Compounds 509 (2011) 9842–9848

Contents lists available at ScienceDirect

Journal of Alloys and Compounds

journal homepage: www.elsevier.com/locate/jallcom

Synthesis, characterization and electrical properties of CdI_2 doped Al_2O_3 and TiO_2 superionic conductors

Saima Sultana, Rafiuddin*

Physical Chemistry Division, Department of Chemistry, Faculty of Science, Aligarh Muslim University, Aligarh 202 002, UP, India

ARTICLE INFO

Article history:
Received 19 May 2011
Received in revised form 22 June 2011
Accepted 23 June 2011
Available online 30 June 2011

Keywords:
Conductivity
Cadmium iodide
Activation energy
Composite
Interface regions

ABSTRACT

Superionic conductors were prepared by admixing metallic oxides (alumina and titania) with cadmium iodide in different proportions using direct mixing method. The synthesized materials were characterized by various qualitative techniques such as XRD (X-ray diffraction), DSC (differential scanning calorimetry) and SEM (scanning electron microscopy). Pure CdI_2 shows the standard pattern which corresponds to β-phase stable at room temperature, however, the diffractograms of the mixtures shows two phase nature of the materials with no effect of the second phase on the peak positions of the first, i.e. CdI_2. DSC curves also confirmed the formation of composite. SEM micrographs show the presence of great number of space charge regions which are very important in creating a great number of surfaces which in turn act as additional sources of point defects. It was also found that the conductivity of CdI_2 increases with mole fractions of dopants till $x = 0.5$ for alumina and $x = 0.3$ for titania. Arrhenius equation was used to study the temperature dependence of electrical conductivity and the activation energy of pure cadmium iodide was found to be 0.792 eV.

1. Introduction

Superionic conductors are those materials which allow macroscopic movement of ions through their structure leading to exceptionally high (liquid-like) values of ionic conductivity while in the solid state. These materials are also known as composite solid electrolytes (CSEs) consisting of an ionic conductor and dispersed insulating phases which can show a dramatic increase in conductivity over that of the pure ionic conductors [1]. The enhancement in conductivity of two phase composite electrolytes was demonstrated for a variety of systems [2–4], and it has become well known that the enhancement is mainly due to enhanced electrical conductivity along the interface layer between the ionic and insulating phases. This enhancement in conductivity is dependent on the composition and microstructures of the CSEs. Conductivity of poor ionic conductors is known to be enhanced by the influence of highly dispersed additives. This influence may either be relatively weak, when bulk physical properties of the ionic salt remain unchanged [5,6], or strong, where interface interaction may lead to formation of composites with new meta stable phases. These meta stable phases could possess unusual bulk properties, including high ionic conductivity [7–9].

Wagner first used the space charge layer concept to explain conductivity effects in semiconducting two phase materials [10]. Liang first revealed the importance of the space–charge layer for the ionic conduction and also suggested the enhancement of ionic conductivity (almost twofold than that of the pure electrolytes) of the electrolyte based composites by admixing fine particles of an inert second phase [1,11,12]. Jow and Wagner [11] attributed this unexpected enhancement to the space–charge region formed near the interface between the matrix electrolyte and the inert second phase.

In most cases, the second phase consists of non-conducting materials such as TiO_2, Al_2O_3, which is nearly insoluble in the host material under the fabrication conditions [13,14]. The conductivity enhancement in composites can be explained in terms of the presence of a greater number of surfaces and interfaces, which act as additional sources of point defect [15]. More recently, the composite effect was also observed in ceramic anion conductors, such as lead or calcium fluoride, or even in inorganic solids with trivalent cationic conductivity, like aluminum and rare-earth wolframates.

Cadmium iodide is an ionic compound, the ionic radii of Cd^{2+} and I^- being ~0.97 and ~2.16 respectively and show strong polarization effects [16]. The structure consists of a hexagonal close-packing of I^- ions with the Cd^{2+} ions distributed among the octahedral

Abbreviations: CSEs, composite solid electrolytes; DSC, differential scanning calorimetry; SEM, scanning electron microscopy; XRD, X-ray diffraction.

* Corresponding author. Tel.: +91 9997005502.
E-mail addresses: saimasultana619@gmail.com (S. Sultana), rafi_amu@rediffmail.com (Rafiuddin).

0925-8388/$ – see front matter © 2011 Elsevier B.V. All rights reserved.
doi:10.1016/j.jallcom.2011.06.102

Nomenclature

C_g	capacitances of grain and grain boundary
E_a	activation energy of ionic motion
k	equilibrium constant
T	temperature
$Z^*(\omega)$	complex impedance
Z'	real impedance
Z''	imaginary impedance
σ_0	pre-exponential factor
τ_g	relaxation time
ω_g	angular frequency of grain

voids in alternate layers. The resultant structure consists of a layered lattice. Cadmium iodide can therefore have five possible space groups — *P*3*ml*, *P*3*rn*, *R*3*m*, *R*3*rn* and *P*63*mc*. Aluminum oxide is a non-conducting (electrical insulator) but has a relatively high thermal conductivity (30 W m^{-1} K^{-1}) for a ceramic material [4]. In its most commonly occurring crystalline form, called corundum or α-aluminum oxide, its hardness makes it suitable for use as an abrasive and as a component in cutting tools.

The aim of the present work is to synthesize and characterize cadmium iodide doped alumina and titania superionic conductors by direct mixing method. Further, the electrical properties of the system as a function of composition as well as temperature have also been studied.

2. Materials and method

2.1. Chemicals

Cadmium iodide was taken from Sigma–Aldrich whereas the titania and alumina were manufactured by BDH Laboratory with the stated purity of 99.9%.

2.2. Sample preparation

The materials (alumina and titania) were first drudged for 2 h with acetone followed by drying at 150 °C for 3 h. These materials were then ground again for an hour and sieved with 200 mesh. The required amount of this material and cadmium iodide were mixed thoroughly using an agate motor and pestle to produce the series $(1-x)\,CdI_2$–xAl_2O_3, x = 0–0.7. The mixtures were then heated in an electrical furnace at 200 °C for 3 h with intermittent grinding. The final mixtures were crushed to fine powders and kept in perfect glass tubes for the analysis.

2.3. Analytical methods

The X-ray diffractograms for the material were recorded using the "BRUKER ADVANCED D8" Diffractrometer with Cuk$_\alpha$ radiations. DSC traces were recorded by heating the mixture in the temperature range 25–450 °C using the PERKIN-ELMER instrument with alumina powder as a reference. The heating rate was kept at 10 °C/min. The electrical conductivity (was measured in the temperature range 373–773 K) and impedance measurement were performed (in the frequency range 42 Hz–5 MHz) using a high tester HIOKI-353250 LCR METER for circular pellets of above material pressed under 4 tonnes/cm^2 pressures. The two opposite surfaces of the pellet were coated with carbon black paint and annealed between the electrodes for 2 h at 150 °C to enhance the electrical connectivity between the samples and the electrodes.

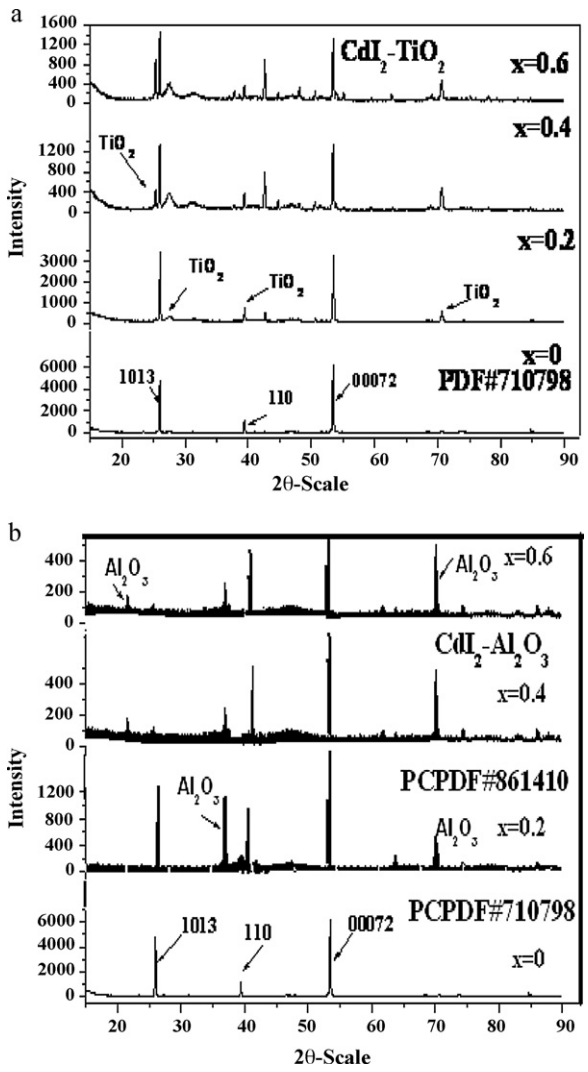

Fig. 1. Room temperature X-ray diffractograms of (a) $(1-x)\,CdI_2$–$xTiO_2$, (b) $(1-x)\,CdI_2$–xAl_2O_3 samples.

3. Results and discussion

3.1. X-ray diffraction

Fig. 1(a and b) shows the X-ray diffractograms of the pure CdI_2 and its mixtures with TiO_2 and Al_2O_3. CdI_2 shows the standard pattern which corresponds to β-phase stable at room temperature. The diffractograms of the mixtures show the two phase nature of these materials with no effect of the second phase on the peak positions of CdI_2. The single phase of CdI_2 has been fitted equally well to the hexagonal polymorph with the rhombo-centered lattice according to the PDF#710798. Additional peaks were observed in Fig. 1(a and b) at x = 0.2, 0.4 and 0.6, which grew up with increasing the mole fraction of titania and alumina. In Fig. 1(a) the additional peaks are attributed to the anatase phase of titania. This phase has been observed to transfer to the rutile phase if titania is sintered at high temperatures or mixed with other impurities [17]. However, in these composites, no indication of the presence of the rutile phase has been detected. In Fig. 1b (2), two additional peaks are observed in the diffractograms, which grow with increasing the mole fraction of aluminum oxide. These are attributed to the cubic phase of alumina. However, the labeled peaks are well characterized to the alumina having monoclinic symmetry with reference to PCPDF#861410. It is worthy to mention that the

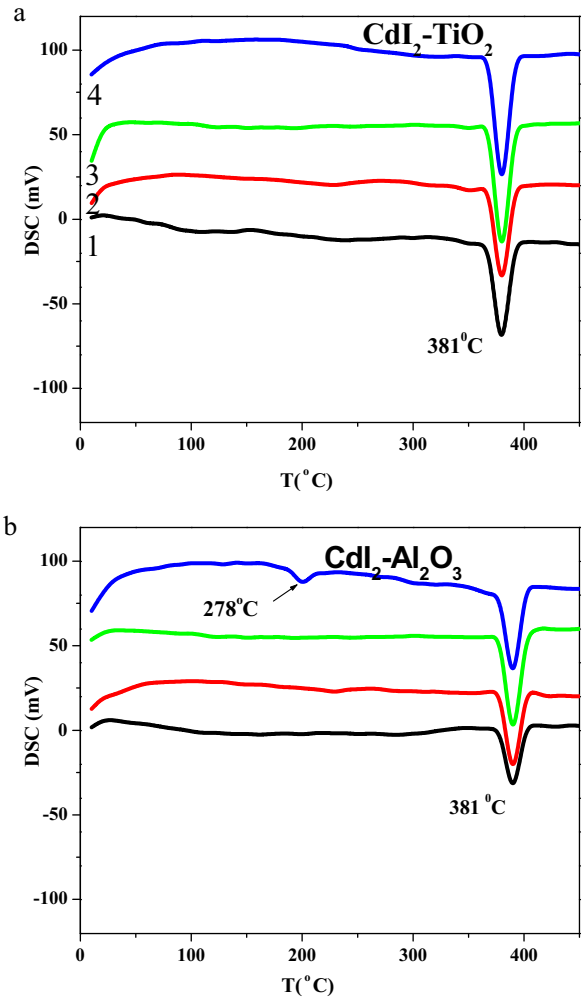

Fig. 2. DSC curves of (a) $(1-x)$ CdI_2–$xTiO_2$, (b) $(1-x)$ CdI_2–xAl_2O_3 samples at different composition (1) $x=0$, (2) $x=0.2$, (3) $x=0.4$ and (4) $x=0.6$.

strong X-ray absorption of CdI_2 causes the intensity of titania and alumina to drop rapidly upon increasing the amount of CdI_2 in the system.

3.2. Differential scanning calorimetry

Fig. 2 shows the heating mode of the DSC curves of the samples taken in the temperature range 25–450 °C. Pure CdI_2 shows the expected behaviour with an intensive peak at 381 °C which is attributed to the melting point. The mixture samples show no appreciable effect on the temperature of the phase transition. However, the peak shifts to the lower side gradually with increasing the mole fraction of the second phase and, in case of alumina doped in CdI_2, a small hump appears at 278 °C on the lower temperature side of the melting peak at 0.6 mol% of alumina. This hump could be due to the formation of an amorphous phase within the space-charge layer that is expected to form between the host material and the dispersoid particles [18,19]. The mixture samples show no appreciable effect on the temperature of the phase transition as observed in the case of: $RbNO_3$–Al_2O_3 [20], CsCl–Al_2O_3 [8], and $Cs_2H_3(SO_4)_4$–SiO_2 [21]. This behaviour has been observed frequently in the ionic salt–oxide composites [20,21]. It has also been noticed that there is no change in the melting point of CdI_2 with increasing the mole fraction of titania and alumina. This is an evidence of the formation of the composite [15].

3.3. Scanning electron microscopy

Fig. 3(a and b) shows the SEM micrographs of two samples, the first one is for pure titania [Fig. 3a (1)] and alumina [Fig. 3b (1)] after the process of its grinding with acetone and then sieving with 200 mesh. The micrograph shows reasonable homogeneity with the average particle size in the range 200–400 nm. The second SEM micrograph [Fig. 3a (2) and Fig. 3b (2)] is for the mixture containing cadmium iodide with 0.4 mol fraction each of titania and alumina, respectively. It provides the information regarding the distribution of the dispersoids (titania and alumina) particles between the particles of cadmium iodide which has a higher average grain size. This distribution of titania and alumina layers between the grains of ionic salt is favored from local thermodynamic equilibrium due to the wetting of alumina and titania particles by CdI_2 grains during the preparation of the mixture [22]. This type of distribution is very important in creating a great number of surfaces which in turn act as additional sources of point defects. This new region between the ionic salt and the added oxide is called the space–charge layer, which strongly alters the bulk properties of the ionic salt [23]. It is also clear that low density and greater number of pores are observed in the mixture sample. This is due to the two phase nature of the sample as well as the particle size difference between the salt and the added oxide as evident from the SEM micrographs.

3.4. Impedance measurements

Complex impedance plots of the investigated samples are shown in Fig. 4(a and b). They are typical plots of ionic conductors showing a semicircle at the high frequency side and a spike towards low frequency. However, the one at higher frequency results from bulk resistance while that at low frequency resulted from grain boundary resistance contribution. It has been found that the idealized impedance plot of such material consists of a semicircle attributed to grain and grain boundary as well as low frequency inclined spike due to the ionic polarization and electrochemical reactions, occurring at the electrode interface [14,24]. The appearance of the spikes is an indication that the conduction in these materials is ionic in nature [16]. These results show the enhancement of ionic conductivity with increase in the dopant amount which is also reflected from the electrical conductivity measurements shown in the figure (Fig. 5).

It is known that the complex impedance $(Z^*(\omega))$ is defined as the sum of its real (Z'') and imaginary part:

$$(Z^*(\omega) = Z' + jZ''; \quad j = \sqrt{-1}) \tag{1}$$

For our modeled equivalent circuit, Z'' and Z' are given as follows:

$$Z' = \frac{R_g}{1+\omega_g^2 C_g^2 R_g^2} \tag{2}$$

$$Z'' = \frac{R_g^2 \omega_g C_g}{1+\omega_g^2 C_g^2 R_g^2} \tag{3}$$

where the resistance of grain (R_g) can directly be obtained from the intercept of the Z'-axis [14]. The angular frequency of grain (ω_g) is obtained at the maxima of the semicircles. As $Z''=Z'$ at the maximum point in the semicircle, the capacitances of grain C_g can therefore be calculated according to Eq. (4).

$$C_g = \frac{1}{R_g \omega_g} \tag{4}$$

The relaxation time τ_g, due to these effects, is obtained from the angular frequency at the maxima using Eq. (5):

$$\tau_g = \frac{1}{\omega_g} = C_g R_g \tag{5}$$

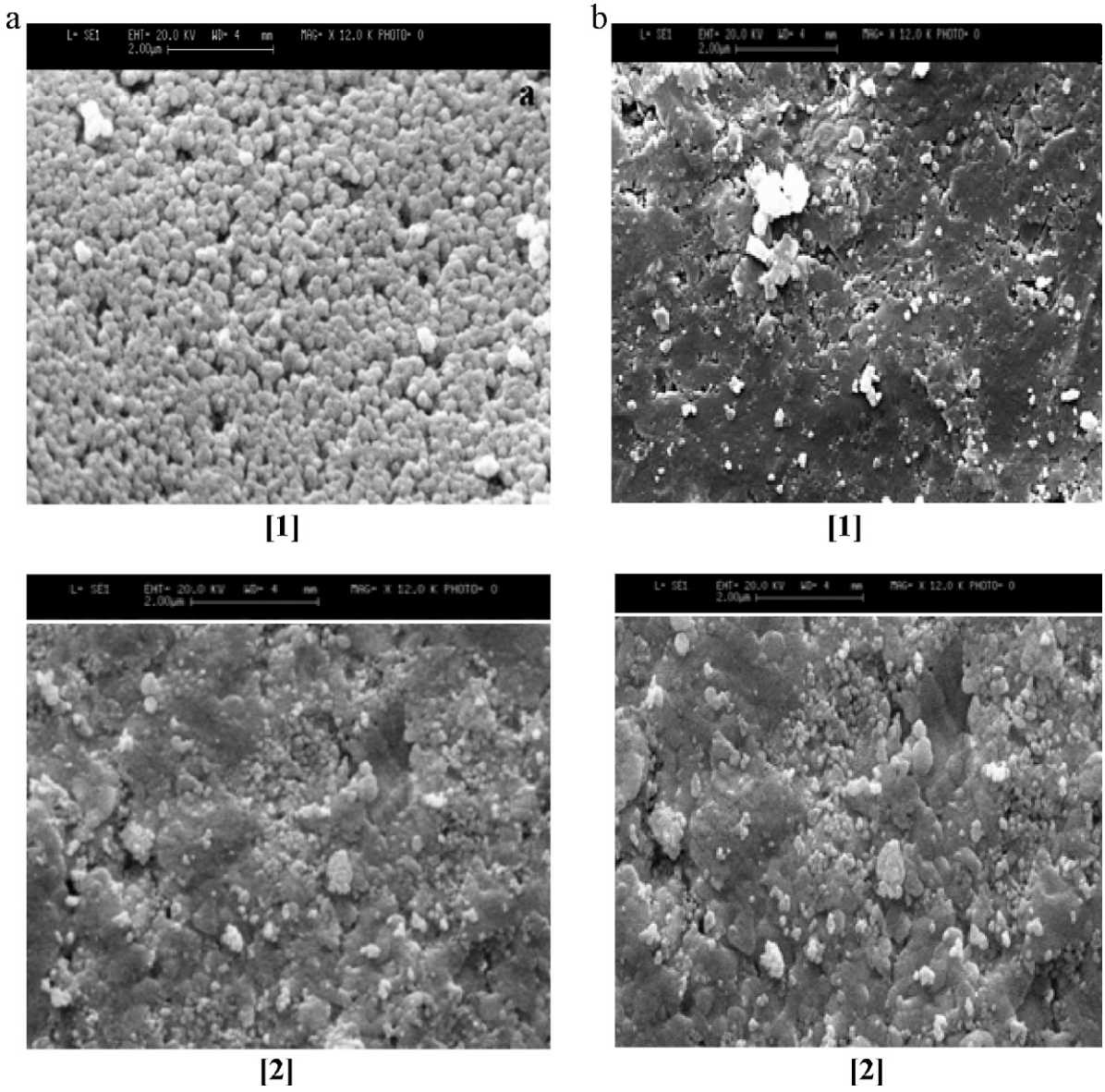

Fig. 3. SEM micrographs of (a) $(1-x)$ CdI_2–$xTiO_2$ samples, (b) $(1-x)$ CdI_2–xAl_2O_3 samples.

But,

$$\sigma = \frac{1}{R_g}$$

So we get,

$$R_g = \frac{1}{\sigma} \tag{6}$$

Substituting Eq. (6) in (5) we get,

$$\tau_g = \frac{1}{\sigma C_g} \tag{7}$$

where σ denotes the conductivity. Eq. (7) implies that relaxation time is inversely proportional to conductivity and in the present study, a decrease in the relaxation time in the systems CdI_2-TiO_2 and CdI_2-Al_2O_3 is observed, which is a clear evidence of the enhancement of ionic conductivity and tabulated in Table 1.

Table 1
Values of the equivalent circuit parameters (R_g, C_g and τ_g) estimated from the impedance spectra for CdI_2-TiO_2 and CdI_2-Al_2O_3 at 25 °C for different mole fractions (x = 0, 0.2, 0.4 and 0.6).

Mole fraction (x)	R_g (kΩ)	C_g (F)	τ_g (s)
CdI_2-TiO_2			
Pure CdI_2	9433.67	5.60×10^{-11}	5.28×10^{-7}
$CdI_{2\,0.8}$-$TiO_{2\,0.2}$	6566.29	6.10×10^{-11}	4.05×10^{-7}
$CdI_{2\,0.6}$-$TiO_{2\,0.4}$	3856.51	7.03×10^{-11}	2.71×10^{-7}
$CdI_{2\,0.4}$-$TiO_{2\,0.6}$	11,539.33	7.10×10^{-12}	0.82×10^{-7}
CdI_2-Al_2O_3			
$CdI_{2\,0.2}$-$Al_2O_{3\,0.2}$	8657.46	6.90×10^{-11}	5.90×10^{-6}
$CdI_{2\,0.6}$-$Al_2O_{3\,0.4}$	24640.87	7.10×10^{-11}	1.75×10^{-6}
$CdI_{2\,0.4}$-$Al_2O_{3\,0.6}$	6370.088	7.50×10^{-11}	4.78×10^{-7}

It was also assumed that τ_g indicates the mean time between two consecutive jumps of a cationic vacancy [14,24].

$$D \propto \frac{\gamma d^2}{\alpha \tau_g} \tag{8}$$

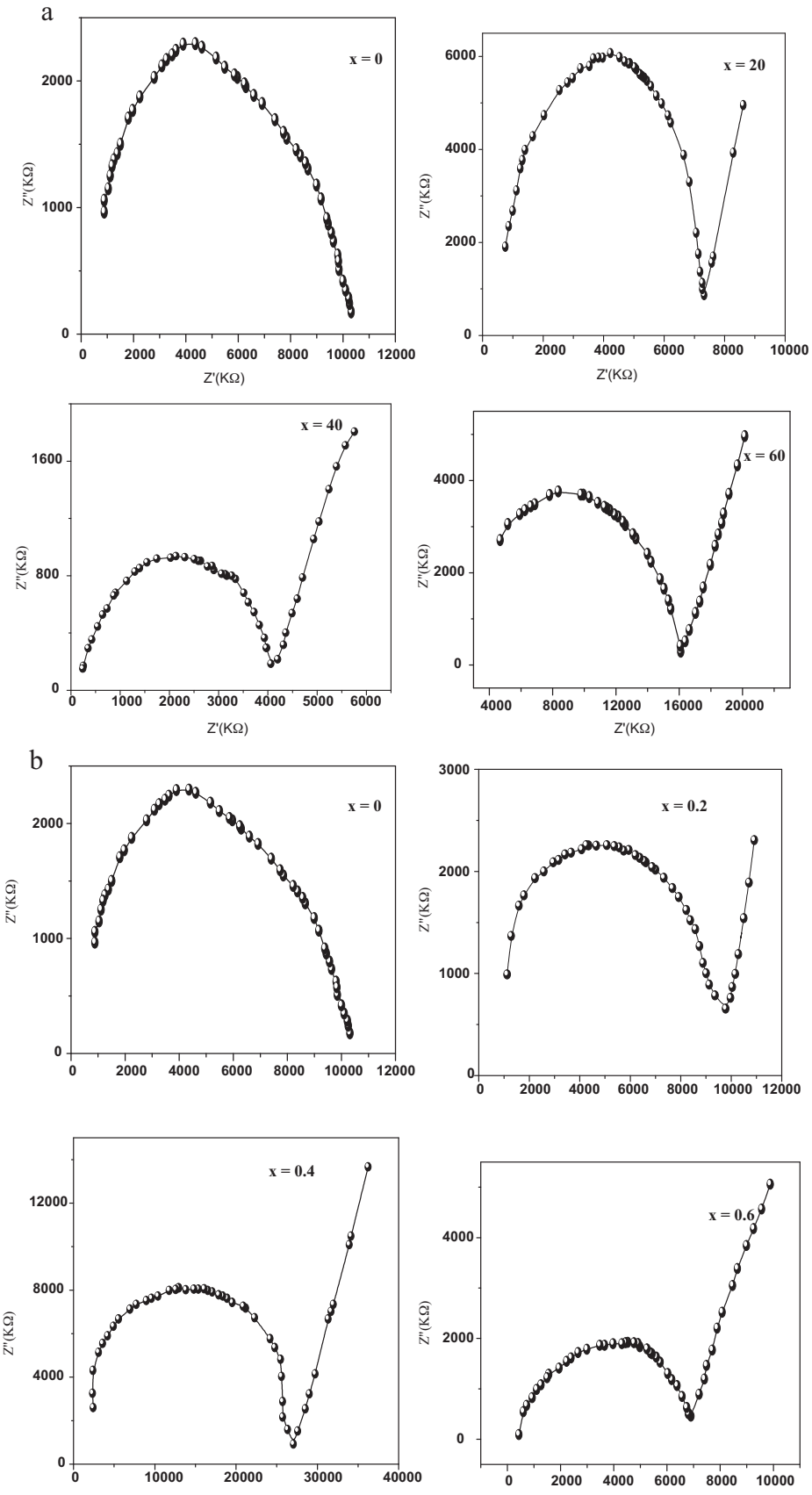

Fig. 4. Impedance spectra of (a) $(1-x)\,CdI_2$–$xTiO_2$ samples, (b) $(1-x)\,CdI_2$–xAl_2O_3 samples.

Alternatively, the diffusion coefficient D is related to relaxation time as follows:

$$D \propto \frac{1}{\tau_g} \tag{9}$$

where d^2 is the mean square jump distance between two adjacent cationic sites in the crystal lattice; γ and α the correlation and geometric factors, respectively. Thus, the shorter the τ is, the faster the cationic diffusion, leading to high ionic conductivity. In the present system, no grain boundary regions are observed.

3.5. Electrical properties

3.5.1. Variation of electrical conductivity with composition

Fig. 5(a and b) illustrates the behaviour of conductivity with the composition of the system at different temperatures. It has been observed from the study that conductivity is directly related to the concentration of the dispersoids, i.e. as the mole fractions of titania or alumina increases, the conductivity increases and passes through a threshold value and thereafter decreases. The threshold value (maxima) is estimated $x = 0.5$ for CdI_2-TiO_2 and $x = 0.3$ for CdI_2-Al_2O_3 systems. The reason behind such high conductivity includes the defect formation to a great extent at the interface region, which itself is a disordered region. When the concentration of the dispersoids exceeds the threshold value in the CdI_2-TiO_2

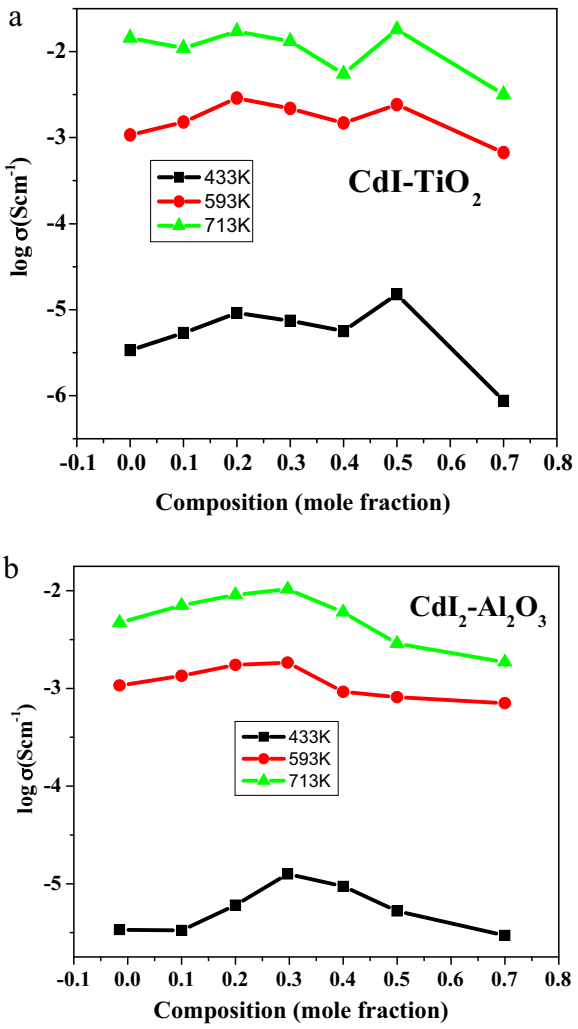

Fig. 5. Electrical conductivity as a function of composition of the (a) $(1-x)$ CdI_2–$xTiO_2$, (b) $(1-x)$ CdI_2–xAl_2O_3 samples at different temperatures.

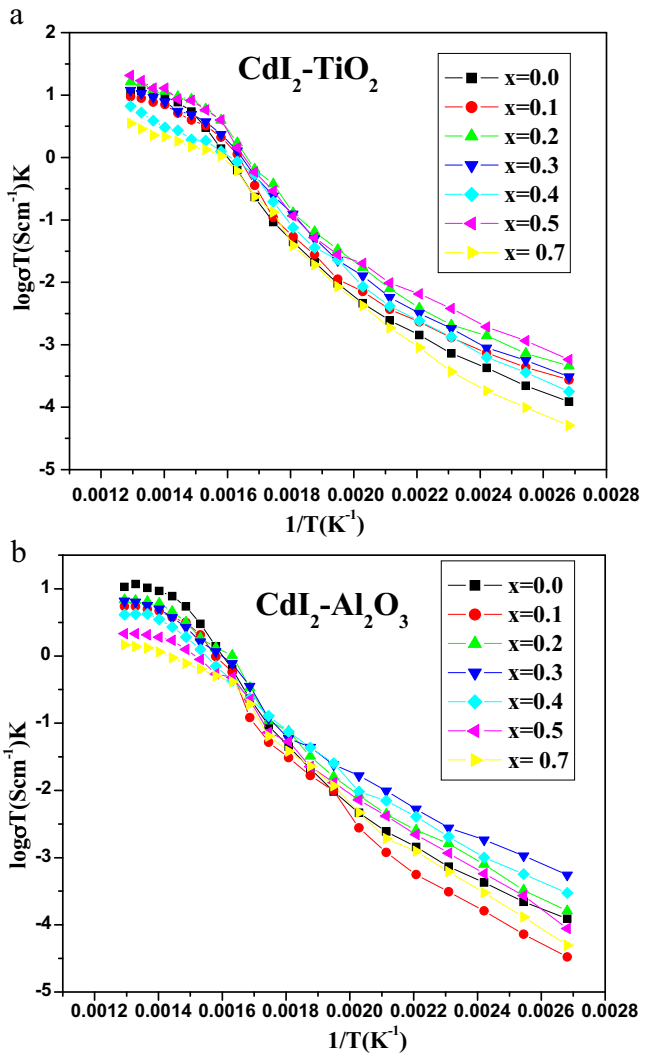

Fig. 6. Electrical conductivity as a function of temperature of the (a) $(1-x)$ CdI_2–$xTiO_2$, (b) $(1-x)$ CdI_2–xAl_2O_3 samples.

($x > 0.5$) and CdI_2-Al_2O_3 systems ($x > 0.3$), the conductivity drops due to the blocking of conduction pathways by the titania and alumina particles [8]. A continuous increase in the contribution of grain boundary towards the total resistivity of the samples is observed with increasing the contents of titania and alumina in the system. This is due to the increase in the phase boundary as reflected from SEM micrographs (Fig. 3a and b).

3.5.2. Variation of electrical conductivity with temperature (Arrhenius equation)

The temperature dependence of ionic conductivity is given by the Arrhenius expression:

$$\sigma T = \sigma_0 \exp\left(\frac{E_a}{kT}\right) \tag{10}$$

where σ_0 is the pre-exponential factor, T is the temperature, k is constant and E_a is the activation energy of ionic motion. The conductivity data were fitted to the above equation in order to obtain the activation energy of conduction. As it is shown in Fig. 6(a and b), two regions are observed in the samples containing titania and alumina amounts up to $x \leq 0.5$ and $x \leq 0.3$ respectively. The activation energies in the temperature range 100–500 °C were calculated using the Linear Regression method and tabulated in Table 2. These values followed the opposite trend of ionic conductivity with the

Table 2
Activation energies of conduction in the temperature range 100–500 °C of the $(1-x)CdI_2$–$xTiO_2$ and CdI_2–xAl_2O_3 samples (evaluated from Arrhenius equation using line fittings).

Mole fraction (x)	Activation energy (eV) TiO_2	Activation energy (eV) Al_2O_3
0	0.792	0.792
0.1	0.730	0.823
0.2	0.729	0.718
0.3	0.721	0.620
0.4	0.695	0.638
0.5	0.703	0.659
0.7	0.756	0.678

composition of the system, i.e. as the conductivity increases the activation energy decreases. The activation energy for pure cadmium iodide was calculated as 0.792 eV which is in quite good agreement with the one reported elsewhere [18].

4. Conclusions

Superionic conductors consisting $(1-x)CdI_2$–$xTiO_2$ and $(1-x)CdI_2$–xAl_2O_3 have been prepared and studied using XRD, DSC, SEM, impedance and electrical conductivity measurements. It has been observed that conductivity has increased two- to three-fold in the composites systems as compared to pure materials. Maximum conductivity were observed in the composition range $x = 0.3$–0.5 mol fraction of the dopants. A general phenomenon behind this seems to be the role played by the interface region which itself is a disordered region where defect formation and migration enthalpies are notably reduced. These disordered regions induce the concentration profile of point defects near the interface region leading to high ionic conductivity. The relaxation time from impedance measurements shows a downward trend with composition throughout the study, which also confirms the enhancement of ionic conductivity.

The appearance of the spikes is an indication that the conduction in these materials is ionic in nature; however, the spike towards the lower frequency range in impedance plots is attributed to the blocking of pathway due to ion migration. Line fittings were used to calculate the activation energy of the samples and it was found to be 0.792 eV for pure CdI_2. Superionic conductors with sufficiently low activation energy (high conductivity) can be produced by present technique for specific applications such as electrical sensors, micro devices used for medical and environmental fields.

Acknowledgements

Authors are thankful to Aligarh Muslim University for providing necessary research facilities. One of the author (Ms Saima Sultana) thanks UGC for providing research fellowship.

References

[1] C.C. Liang, J. Electrochem. Soc. 120 (1973) 1289.
[2] L. Chen, in: B.V.R. Chowdhri, S. Radhakrishna (Eds.), Material for Solid Batteries, World Scientific, Singapore, 1986, p. 69.
[3] J.B. Wagner Jr., in: T. Takahashi (Ed.), High Conductivity Solid Ionic Conductors, World Scientific, Singapore, 1989, p. 69.
[4] N.J. Dudney, Annu. Rev. Mater. Sci. 19 (1989) 103.
[5] J. Maier, J. Phys. Chem. Solids 46 (1985) 309.
[6] N.F. Uvarov, J. Maier, Solid State Ionics 62 (1993) 251.
[7] L. Chen, Materials for Solid State Batteries, World Scientific, Singapore, 1989.
[8] N.F. Uvarov, V.P. Isupov, B.B. Bokhonov, E.F. Hairetdinov, Solid State Ionics 74 (1994) 15.
[9] B. Wassermann, T.P. Martin, J. Maier, Solid State Ionics 28 (1987) 1514.
[10] C. Wagner, J. Phys. Chem. Solids 33 (1972) 1051.
[11] T. Jow, J.B. Wagner Jr., J. Electrochem. Soc. 126 (1979) 1963.
[12] A.R. Verma, P. Krishna, Polymorphism and Polymorphism in Crystals, Wiley, New York, 1966, Russian translation edited by A. S. Povarennykh MIR: Moscow (1969).
[13] S. Sultana, R. Uddin, Physica B 404 (2009) 36–40.
[14] S. Sultana, R. Uddin, Ionics 15 (2009) 621–625.
[15] N.F. Uvarov, P. Vanek, Yu.I. Yuzyuk, V. Zelenzy, V. Studnika, B.B. Bocknonov, V.E. Dutepov, J. Peptzept, Solid State Ionics 90 (1996) 201.
[16] V. Thangaduarai, H. Kaack, W. Wepper, J. Am. Ceram. Soc. 86 (2003) 437.
[17] A.M.M. Farea, S. Kumar, K.M. Batoo, A. Yousef, C.G. Lee, Alimuddin, J. Alloys Compd. 464 (2008) 361.
[18] S. Sultana, R. Uddin, Arab. J. Chem., doi:10.1016/j.arabjc.2011.02.025, in press.
[19] M.V. Madhava Rao, et al., Physica B 362 (2005) 193.
[20] J.W. Brightwell, C.N. Buckley, L.S. Miller, B. Ray, Phys. Status Solidi (A) 76 (2006) 391.
[21] S. Popovic, Z. Skoko, A. Gajovic, K. Furic, S. Mustic, Fizika A 14 (2005) 19.
[22] G.V. Lavrova, V.G. Ponomareva, E.B. Burgina, Solid State Ionics 176 (2005) 767.
[23] J.R. Dygas, M. Malys, F. Krok, W. Wrobel, A. Kozanecka, I. Abrahams, Solid State Ionics 176 (2005) 2085.
[24] M.J. Godinho, P.R. Bueno, M.O. Orlandi, E.R. Leite, E. Long, Mater. Lett. 57 (2003) 2540.